Journal of
Materials Chemistry A

Materials for energy and sustainability

Accepted Manuscript

This article can be cited before page numbers have been issued, to do this please use: E. Sánchez-Ahijón, R. Marín-Gamero, B. Molero-Sánchez, D. Ávila-Brande, A. Manjón-Sanz, M. T. Fernandez-Diaz, E. Morán, R. Schmidt and J. Prado-Gonjal, *J. Mater. Chem. A*, 2020, DOI: 10.1039/C9TA12208G.

ROYAL SOCIETY OF CHEMISTRY

rsc.li/materials-a

View Article Online
DOI: 10.1039/C9TA12208G

ARTICLE

From theory to experiment: $BaFe_{0.125}Co_{0.125}Zr_{0.75}O_{3-\delta}$, a highly promising cathode for intermediate temperature SOFCs

Received 00th January 20xx,
Accepted 00th January 20xx

DOI: 10.1039/x0xx00000x

Elena Sánchez-Ahijón,[a] Rafael Marín-Gamero,[a] Beatriz Molero-Sánchez,[b] David Ávila-Brande,[a] Alicia Manjón-Sanz,[c] M.Teresa Fernández-Díaz,[d] Emilio Morán,[a] Rainer Schmidt,[e] Jesús Prado-Gonjal*[a,f]

In a recent theoretical study [Jacobs et al. Adv.Energy Mater. 2018, **8**, 1702708], $BaFe_{0.125}Co_{0.125}Zr_{0.75}O_{3-\delta}$ was predicted to be a stable phase with outstanding performance as an auspicious cathode for intermediate-temperature solid oxide fuel cells (IT-SOFCs). It is shown here that the theoretical predictions are valid. The material can be synthesized by the citrate method as a single cubic $Pm\bar{3}m$ phase with a significant amount of oxygen vacancies, randomly distributed in the anionic sublattice facilitating oxygen vacancy conduction. A thermal expansion coefficient of 8.1 x 10^{-6} K^{-1} suggests acceptable compatibility with common electrolytes. Electrochemical impedance spectroscopy of symmetrical cells gives an area-specific resistance of 0.33 Ω·cm² at 700 °C and 0.13 Ω·cm² at 800 °C . These values are reduced to 0.13 Ω·cm² at 700 °C and 0.05 Ω·cm² at 800 °C when the material is mixed with 30%wt of $Ce_{0.9}Gd_{0.1}O_{2-\delta}$. Consider to use the acronym BFCZO more often.

Introduction

A solid oxide fuel cell (SOFC) is an electrochemical device that converts chemical into electrical energy via electrochemical reactions. [1-4] It consists of a highly dense and oxygen ion conducting electrolyte, which is sandwiched between an anode and a cathode, both with a substantial porosity. The oxidation of a fuel (H_2, CO, CH_4) at the anode produces an excess of electrons, which move through an external circuit to the cathode, where the reduction of oxygen molecules requires electrons. Optimizing the components for these devices (electrodes and electrolyte) and lowering the operating temperature of SOFCs to the intermediate range (500 – 750 °C) are the main aspirations in this field of research.[5-8]

Mixed ionic and electronic conductors (MIECs) are considered auspicious candidates as cathodes for these intermediate temperature solid oxide fuel cells (IT-SOFCs).[9, 10] The presence of ionic and electronic conductivity simultaneously and the movement of electrons from the external circuit to the cathode surface promote oxygen reduction. The ionic conductivity facilitates the O^{2-} movement from the triple phase boundary (TPB) to the electrolyte, while the electronic conductivity contributes to the transfer of electrons from the external circuit to the TPB, where the electrochemical reaction takes place. For an efficient cell performance, it is particularly important to increase the number of active sites for the oxygen reduction reaction (ORR) on the cathode surface. This is achieved by the increase of the specific surface area accessible for the conversion of oxygen molecules to oxygen anions.[11-13] Furthermore, for the reduction of ohmic losses at the electrode, it is crucial to find a material with high electrical conductivity and area-specific resistance (ASR) lower than 0.15 Ω cm^2 at the application temperature, or to prepare a composite by mixing an ionic with an electrical conductor.[5, 14, 15] Additionally, mechanical and chemical compatibility with similar thermal expansion coefficient (TEC) between the electrode and the electrolyte materials are essential. Typical SOFC electrolytes, such as yttria-stabilized zirconia (YSZ) and gadolinium-doped ceria (GDC) possess values of TEC ≈ 10 – 12 x 10^{-6} K^{-1}.[16] Delamination at the solid-solid interfaces or stress of the cell can occur if there is a too large divergence between the TEC values of the components.[9, 17] Previous studies suggest that a difference in the thermal expansion coefficient of the components of the cell of ≈ 7 x 10^{-6} K^{-1} is sufficient to produce degradation.[18]

In the search for new cathode materials for SOFCs, perovskite-based oxides offer an impressive versatility in chemical composition, structural tolerance to oxygen vacancies, chemical stability and the possibility of tuning the transport properties by substitution or introduction of defects. Among them, Co-based and Mn-based perovskites are most frequently used. [19-22] Some examples of typical cathodes for SOFC are $La_{1-x}Sr_xCoO_{3-\delta}$,[23] $La_{1-x}Sr_xMnO_{3-\delta}$,[24, 25] $La_{1-x}Sr_xCr_{0.5}Mn_{0.5}O_{3-\delta}$,[26] $SrCo_{1-x}Fe_xO_{3-\delta}$,[27] $Sm_xSr_{1-x}CoO_{3-\delta}$,[28, 29] $Ba_{0.5}Sr_{0.5}Co_{1-x}Fe_xO_{3-\delta}$ [30, 31] or $La_{2-x}Sr_xCoO_{4-\delta}$.[32, 33] These perovskites are usually synthesized by the ceramic method, involving multiple heating and regrinding steps. However, there is a noticeable interest in the

[a] Dpto. Química Inorgánica, Universidad Complutense de Madrid, E-28040 Madrid (Spain)
[b] SeeO2 Energy Inc, 3655 36 St NW, Calgary, AB T2L 1Y8, Canada
[c] CELLS–ALBA synchrotron, Cerdanyola del Vallés, Barcelona, E-08290 (Spain)
[d] Institute Laue Langevin, BP 156X, Grenoble F-38042, France
[e] GFMC, Dpto. Física de Materiales, Facultad de Ciencias Físicas, Universidad Complutense de Madrid, E-28040 Madrid (Spain)
[f] Instituto de Ciencia de Materiales de Madrid (ICMM), Consejo Superior de Investigaciones Científicas (CSIC), Sor Juana Inés de la Cruz 3, E-28049, Madrid, Spain
* corresponding author: jpradogo@ucm.es

Electronic Supplementary Information (ESI) available: [details about synchrotron X-ray diffraction, neutron diffraction, powder X-ray thermodiffraction, thermal expansion coefficient, impedance spectroscopy of the cells]. See DOI: 10.1039/x0xx00000x

development of "soft chemistry" and "fast chemistry" routes for the preparation of materials for SOFCs.[34-36] These alternative methods, - such as combustion, microwave-assisted synthesis, sol-gel, - help to minimize the reaction time and temperature of the reaction, facilitating the formation of nanoparticles with a high specific surface area.[37-40]

Recently, *Jacobs et al.* [41] published a computational study where 2145 distinct perovskite phases were screened for potential industrial use as high activity cathodes for SOFCs. By applying several filters (high surface exchange coefficient *k**, chemical stability under ORR operating conditions, adequate band and charge transfer gaps, low cost of constituent atoms), Jacobs et al. suggested 3 top materials. Among them, the $BaFe_{0.125}Co_{0.125}Zr_{0.75}O_3$ perovskite was suggested, which was selected here due to inexpensive reactants and a simple synthesis procedure. The material exhibits a calculated oxygen *p*-band center of -1.355 eV and a low surface exchange coefficient (log k^* = -2.779 cm s^{-1}), where the latter connects with high cathode ORR activity. The position of the bulk O *p*-band center relative to the Fermi level correlates strongly with the oxygen surface exchange kinetics.[41, 42]

Here, we report on the synthesis of $BaFe_{0.125}Co_{0.125}Zr_{0.75}O_{3-\delta}$ (BFCZO) by the citrate route, structural and microstructural characterization, and the electrochemical performance of (1) the sintered material, (2) a symmetrical cell containing BFCZO/GDC/BFCZO and (3) a symmetrical cell containing BFCZO:GDC/GDC/BFCZO:GDC. Impedance spectroscopy data from a sintered pellet of BFCZO suggest mixed conductivity, while the analysis of the results for the symmetrical cells in a 2-electrode configuration reveals promising ASR_p values for the use of this material as a cathode in IT-SOFCs.

Experimental

Synthesis, sintering and symmetrical cell fabrication:

$BaFe_{0.125}Co_{0.125}Zr_{0.75}O_{3-\delta}$ perovskite was prepared as polycrystalline powder by the citrate method. Stoichiometric amounts of inexpensive starting chemicals $Ba(NO_3)_2$ (Sigma-Aldrich, 99 %), $Fe(NO_3)_3 \cdot 9H_2O$ (Sigma-Aldrich, 99.95%), $Co(NO_3)_2 \cdot 5.41\ H_2O$ (Sigma-Aldrich, 99.999%) and $ZrO(NO_3)_2 \cdot 6H_2O$ (Sigma-Aldrich, 99 %) were dissolved in a citric acid solution, which was slowly heated (80 °C), under constant stirring, until the evaporation of the solvent and the formation of a sponge-like precipitate. The precipitate was calcined at 1100 °C for 12 h.

The resulting powder was compacted into pellets, using a 2 ton die press for 5 min. Pressure-less sintering was performed in air at 1200°C for 12 h. For the electrical characterization by impedance spectroscopy, the pellet surfaces were first thoroughly polished and then covered on both sides with Au electrodes using dc sputtering. Symmetrical cells were prepared by depositing layers of slurries, containing BFCZO powder or BFCZO:GDC (70:30 wt %) composites and DecofluxTM binder, onto both sizes of a commercial GDC (Fuel Cells Materials) pellet (1 mm thickness, 10 mm diameter, density ≈ 97 %). The cells were annealed at 980 °C for 3 h in air, with a heating and cooling rate of 2.5 °C/min. Silver paste was used as a current collector.

Structural and microstructural characterization:

Synchrotron X-ray diffraction (SXRD) of the powders was performed at room temperature using the BL04-MSPD beamline at ALBA synchrotron (Barcelona, Spain).[43] The MYTHEN detector and an incident beam with energy of 28.5 keV (λ = 0.4349 Å) were used for the experiment. The diffractogram was collected in a rotating glass capillary of 0.5 mm diameter containing the sample to improve diffracting particle statistics covering an angular range from 3° to 40°. The exposure time was 5 min.

Neutron powder diffraction (NPD) data from room temperature to 700 °C, were collected at the D2B beamline at the Institut Laue Langevin (ILL), Grenoble, using a wavelength of 1.549 Å within the angular range 2θ of 5-150°. This experiment facilitates the decoupling of the thermal and occupancy factors, allows the determination of the oxygen content and the possible cation ordering in the structure, as there is a significant divergence in the neutron scattering lengths of the constituent elements of the sample [Ba (5.07 fm), Fe (9.45 fm), Co (2.49 fm), Zr (7.16 fm) and O (5.80 fm)]. Room-temperature NPD data were collected during 6 h for a 2.5 g sample, packed in a cylindrical vanadium can, in the high-intensity mode. Furthermore, NPD patterns were also collected at 300, 500 and 700 °C. In this case, the sample was contained in a quartz tube in air.

Structural Rietveld refinements of both the synchrotron and neutron data sets were carried out using Fullprof software.[44] Pseudo-Voigt peak shapes were used for the analysis. Scale factor, background coefficients, zero-point error, asymmetry parameters, atomic positions, occupancy of the constituent elements, isotropic atomic displacements for the cations and anisotropic atomic displacements for the oxygen were refined.

Thermogravimetric analysis of a 50 mg sample was performed in a Q600 TA Instruments, from room temperature to 800 °C, working in air flow at a heating rate of 5 °C/min.

High resolution transmission electron microscopy (HRTEM) for BFCZO powder was performed using a JEOL 3000F microscope. Images were recorded with an objective aperture of 70 µm centered on a sample spot within the diffraction pattern area. Fast Fourier Transforms (FFTs) of the HRTEM images were carried out to reveal the periodic image contents using the Digital Micrograph package. This microscope is equipped with an EDAX Inc. energy-dispersive X-ray detector for microanalysis.

The microstructure of the symmetrical cells after electrochemical testing were examined by scanning electron microscopy (SEM) on a JEOL 6700 microscope

Electrochemical characterization:

Solid state impedance spectroscopy (IS) measurements on a sintered pellet were carried out at 160-540 K using a Novocontrol Alpha-A High Performance Frequency Analyzer, equipped with a liquid nitrogen cooled sample chamber. A 100 mV amplitude alternating voltage signal was employed and IS data was obtained at each temperature in terms of the real and imaginary parts of the impedance (Z'–Z'') at various frequencies (f) between 1 Hz and 10 MHz. The impedance spectra were fitted using Zview software. The total electrical *dc* resistivity of dense rectangular bars was determined by a four-probe method in air. Measurements were performed in an Autolab PGSTAT302N in galvanostatic mode from 50 °C to 900 °C in steps of 50 °C and in a current range 0-100 mA.

View Article Online
DOI: 10.1039/C9TA13208G

Cell testing: Electrochemical impedance spectroscopy (EIS) was carried out on the symmetrical cells to test the electrochemical performance of BFCZO as a cathode material for SOFCs. Data were taken in a 2-electrode symmetrical cell configuration in stagnant air on heating and cooling cycles at temperatures of 500 °C, 550 °C, 600 °C, 650 °C, 700 °C, 750 ºC and 800 ºC using a Solartron 1255 analyser. In this case, a 50 mV amplitude alternating voltage signal was employed with a frequency range of 0.5 Hz - 3 MHz. Area-specific resistance (ASR) values were determined by means of the typical procedure for symmetrical cells: extracting the electrolyte and measuring-device resistances, correcting for the electrode area and dividing by 2.[9, 45, 46]

Results and discussion

Structural and microstructural characterization:

Combined SXRD and NPD pattern were used to determine the crystallographic structure of $BaFe_{0.125}Co_{0.125}Zr_{0.75}O_{3-\delta}$ at room temperature. Figure 1 shows the Rietveld refinement of the SXRD data. Typical reflections of the cubic $Pm\bar{3}m$ (#221) space group are observed in the diffractogram. Details about SXRD results are summarized in the electronic supplementary information SI1. A small amount of the secondary phase $BaZrO_3$ (< 4%), which also crystallizes in $Pm\bar{3}m$ is not visible by laboratory X-ray diffraction, but can be observed in the SXRD data.

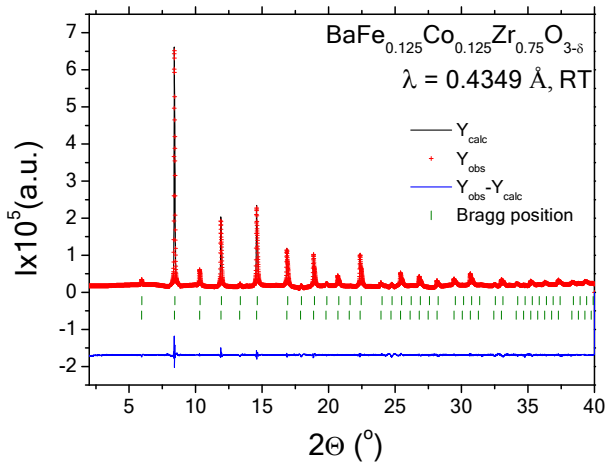

Figure 1. Observed (red crosses), calculated (black, full line), and difference (blue line) synchrotron x-ray diffraction profile for BFCZO sample at room temperature. Bragg reflections are marked in green bars.

The chemical stability of $BaFe_{0.125}Co_{0.125}Zr_{0.75}O_{3-\delta}$ perovskite under heating was determined by *in situ* NPD (Figure 2). The cubic structure is preserved and only the characteristic shift of the reflection towards lower angles is perceived, indicating a thermal expansion of the unit cell parameters.

Table 1 summarizes the lattice parameters, occupancies, thermal parameters, selected atomic distances and agreement factors of the NPD refinements. Ba atoms occupy 1*b* Wyckoff position (0.5, 0.5, 0.5) while Fe, Co and Zr share 1*a* Wyckoff position (0, 0, 0) and oxygen atoms are located on 3*d* Wyckoff position (0.5, 0, 0). No additional reflections are present, so there is no evidence of any superstructure arising from the long range ordering of cations or oxygen vacancies.

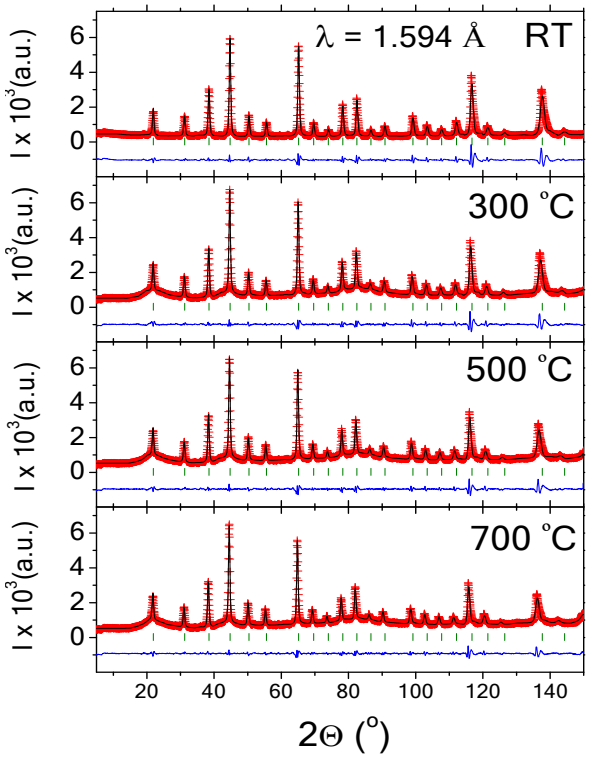

Figure 2. Observed (red crosses), calculated (black, full line) and difference (blue line) NPD profiles for $BaFe_{0.125}Co_{0.125}Zr_{0.75}O_{3-\delta}$ at room temperature, 300, 500 and 700◦C in air. The vertical green bars correspond to the allowed Bragg reflections.

It should be considered at this point that there is a remarkable number of oxygen vacancies, randomly distributed in the anionic sublattice, giving an experimental formula at room temperature of $BaFe_{0.13(1)}Co_{0.13(1)}Zr_{0.74(1)}O_{2.90(2)}$, which facilitates oxygen vacancy conduction. Furthermore, the anisotropic atomic displacement analysis of oxygen atoms reveals disk-shaped ellipsoids, having the shorter diameter directed along the Transition Metal-Oxygen bond (illustration of the structure with the thermal ellipsoids is shown in the electronic supplementary information SI2). This arrangement is typical of MIECs perovskites.[34, 35] In this case, the vibration of the oxygen has a preferential effect in the plane perpendicular to the Fe, Co and Zr atoms.

Temperature dependent NPD data collected in air yields a decrease of the oxygen content with increasing temperature with a minimum of $BaFe_{0.13(1)}Co_{0.13(1)}Zr_{0.74(1)}O_{2.86(1)}$ at 700 °C. This effect, combined with the increase of the thermal parameters during heating, may be beneficial for the oxygen ion diffusion, i.e. increasing the number of active sites for the oxygen reduction reaction (ORR) and improving the ionic conductivity, which is indispensable for the application in IT-SOFCs. It should be noted that the phase remains stable at high temperature as predicted by Jacobs et al. [41]

The thermal expansion coefficient determined from the variation of the cell parameters correspond to 8.1×10^{-6} K^{-1} in

View Article Online
DOI: 10.1039/C9TA13208C

the range from room temperature to 700 °C. This result suggests reasonable compatibility with common electrolytes, such as gadolinium-doped ceria or yttria-stabilized zirconia (YSZ), which possesses values of TEC between ≈ 10 – 12 x 10^{-6} K^{-1}.[16] Conventional X-ray thermodiffraction data are in good agreement with these results (Supplementary Information SI3).

Table 1: Refined structural parameters obtained from NPD for $BaFe_{0.125}Co_{0.125}Zr_{0.75}O_{3-\delta}$ from room temperature (RT) to 700 °C.

T (°C)	RT	300	500	700
Lattice parameter, a / Å	4.1863(1)	4.1942(1)	4.2003(1)	4.20773(9)
Occ. Ba (0.3333)	0.3333	0.3333	0.3333	0.3333
Occ. Fe (0.0418)	0.042(5)	0.042(5)	0.042(5)	0.042(5)
Occ. Co (0.0418)	0.044(5)	0.044(5)	0.044(5)	0.044(5)
Occ. Zr (0.2497)	0.248(5)	0.248(5)	0.248(5)	0.248(5)
Occ. O (1)	0.966(7)	0.964(7)	0.956(5)	0.953(4)
B_{iso} (Ba) / $Å^2$	1.17(4)	1.53(4)	1.90(4)	2.27(4)
B_{iso} (Fe/Co/Zr) / $Å^2$	0.91(3)	0.99(3)	1.17(4)	1.36(3)
β_{11} x 10^4 (O) / $Å^2$	136(9)	165(9)	171(9)	209(9)
β_{22} x 10^4 (O) / $Å^2$ *	231(6)	295(6)	354(7)	443(6)
d (Fe/Co/Zr)-O / Å	2.09318(6) x 6	2.09715(6) x 6	2.10019(6) x 6	2.10387(5) x 6
d Ba-O / Å	2.96020(6) x 12	2.96582(6) x 12	2.97012(6) x 12	2.97533(5) x 12
R_p (%)	6.30	3.76	3.20	2.85
R_{wp} (%)	8.60	5.46	4.69	3.97
R_{exp} (%)	1.35	1.59	1.61	1.58
Bragg R-factor	1.92	1.74	1.84	1.46
Anisotropic β O: * $\beta_{22} = \beta_{33}$; $\beta_{12} = \beta_{23} = \beta_{13} = 0$				

Thermogravimetric analysis (TGA) confirms the weight loss when heating the sample, associated to the corresponding decrease of the oxygen content (Figure 3). From room temperature to 700 °C (application temperature), there is a weight loss of ≈ 0.45%, which, assigning the totality of the losses to the oxygen content variation, it would correspond to an experimental formula of $BaFe_{0.13}Co_{0.13}Zr_{0.74}O_{2.80}$, not far from the result found in the NPD refinement at the same temperature ($BaFe_{0.13(1)}Co_{0.13(1)}Zr_{0.74(1)}O_{2.86(1)}$). There is no variation of the XRD pattern of $BaFe_{0.125}Co_{0.125}Zr_{0.75}O_{3-\delta}$ after TGA in air and phase decomposition can be excluded.

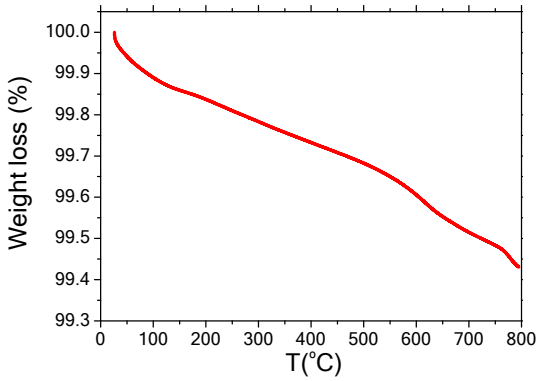

Figure 3. Thermogravimetric analysis (TGA) in air of $BaFe_{0.125}Co_{0.125}Zr_{0.75}O_{3-\delta}$

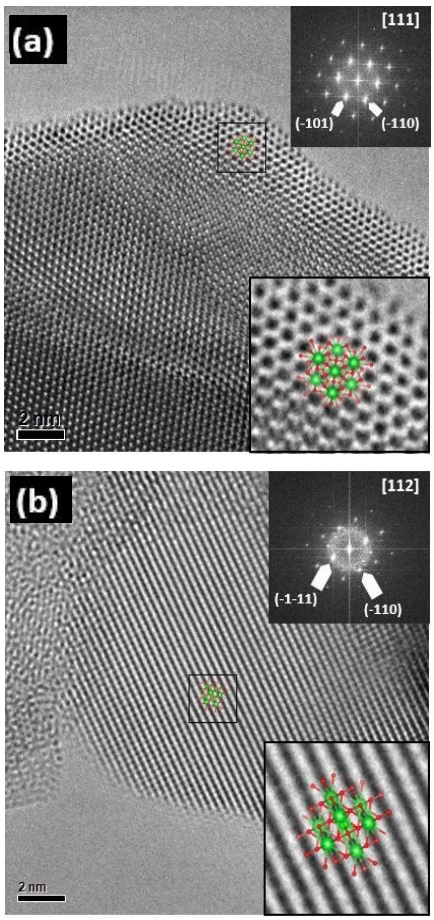

Figure 4. HRTEM images along (a) [111] and (b) [112] zone axes. FFT images are shown in the upper inset, with no evidence of streaking or extra spots. Bottom insets correspond to the enlargement of the areas squared in black with the projected structural model over imposed.

Figure 4 shows the HRTEM micrographs taken along the [111] and [112] zone axes. In the images, the black dots correspond to the projections of the atomic columns from the cationic Ba and Fe/Co/Cr sublattices, showing well-ordered crystals without the formation of superstructures or defects. This is evidenced by a regular contrast across the HRTEM images and the absence of extra spots or streaking lines in the FFTs (Figure 4a,b upper insets).
Enlargements of the experimental HRTEM images displayed at the bottom left part show a good agreement between the contrast and the location of the cations.

Electrochemical properties of the sintered pellets:

Impedance spectroscopy data for $BaFe_{0.125}Co_{0.125}Zr_{0.75}O_{3-\delta}$ were collected from a sintered pellet (density ≈ 85%) and analysed using Zview software.[47] A representative impedance spectrum at 280 K is presented in Figure 5a in terms of the complex impedance plane plot of −Z″ vs Z′.[48, 49] The sample shows only one dielectric contribution associated with the bulk. No grain boundary (GB) contribution is evident in the complex impedance spectrum. The detected single semicircle is highly supressed and in fact the dielectric relaxation peaks are asymmetric. This can be seen clearly in Figure 5b, where the modulus plots of M" (dimensionless) are presented vs frequency f (Hz). These asymmetric relaxation peaks are typical for ionic conductors and may be considered a clue for the presence of ionic conductivity in the sample. Although M" vs f (Figure 5b) does not show a second peak, the data can be fitted satisfactorily only with the circuit shown in the Figure 5a inset, consisting of one ideal and one non-ideal RC element in series. However, the two RC elements are not independent from each other and the bulk resistance is given by R1 + R2, i.e. the semicircle diameter. The equivalent circuit has been used before for ionic conductors displaying non-symmetric bulk dielectric relaxation peaks in M″ vs f.[50]

Figure 6 shows the resistivity of the sample plotted on a logarithmic scale vs 1/Temperature. Low temperature results were extracted from R1 + R2 and the pellet normalization. There is a good agreement between the impedance spectroscopy and 4-point method resistivity results in the matching temperature zone. The small offset between the two curves is attributed to mainly the uncertainty in the geometric factor and to a lesser degree to the precision of the thermometers. The electrical resistivity of BFCZO at 700 ºC is ≈ 1.1 Ω cm. The substitution of Zr for a higher amount of Co would produce an increment of the electronic conductivity.[51] On the other hand, certain drawbacks appear in SOFC cathodes if the content of cobalt increases, such as a high chemical reactivity with the electrolyte and limited structural stability at high temperature (easy evaporation and diffusion). Furthermore, the thermal expansion coefficient is affected due to the Co redox behaviour.[52]

The activation energy (E_A) of the material is determined from the slope in the linear regime, using the Arrhenius´ equation (Figure 6). The activation energy of the process obtained from IS data (E_A) is 0.32 eV, which is in good agreement with the E_A value found from room temperature to 350 **°C** in the 4-point resistivity measurement (E_A = 0.38 eV). However, an electrical transition is visible at T>350 **°C**, achieving an E_A of 0.21 eV for this high temperature regime. These values are not far from E_A found for other $BaZrO_3$-doped materials, such us 10% Y-doped $BaZrO_3$ (E_A = 0.42 eV).[53]

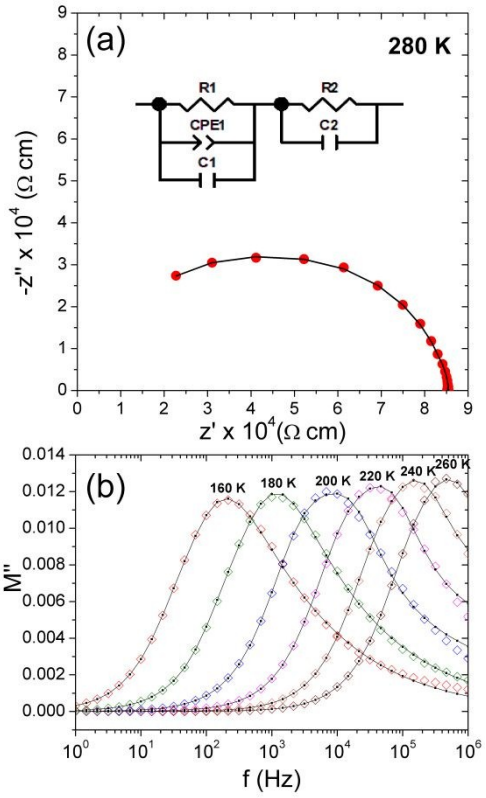

Figure 5. (a) Plot of the imaginary versus real part of the impedance (−Z″ vs Z′) at 280 K. Red circles correspond to the experimental data while the black line represents equivalent circuit fits using the model shown in the figure. (b) Modulus M″ vs frequency plot from 260 K to 160 K. Open symbols represent measured data, black squares and solid lines represent equivalent circuit fits using the model shown.

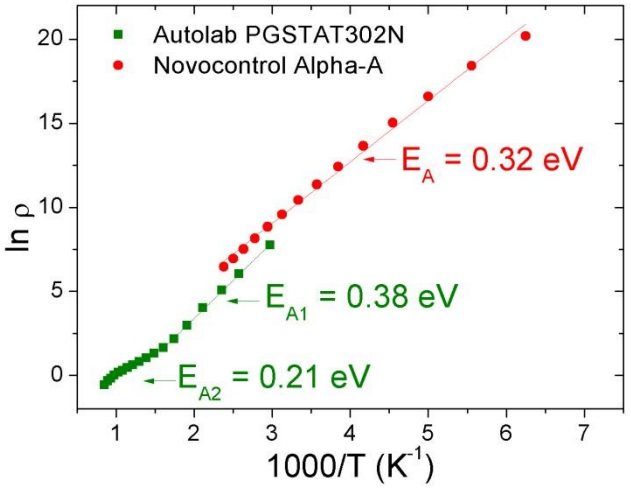

Figure 6. Temperature dependence of the $BaFe_{0.125}Co_{0.125}Zr_{0.75}O_{3-\delta}$ resistivity ρ. Red circles represent the data determined from the Novocontrol Alpha-A instrument, while green squares correspond to the total electrical resistivity measured by the 4-point method using the Autolab instrument. Solid lines represent the linear fit of the data on Arrhenius axes.

Symmetrical cells

Before studying the electrochemical properties of the symmetrical cells, the chemical compatibility of $BaFe_{0.125}Co_{0.125}Zr_{0.75}O_{3-\delta}$ with the electrolyte (GDC) was verified by laboratory XRPD, heating a mixture of 70 %wt of the perovskite phase with 30 %wt of GDC at 980 °C for 24 h, but there was no evidence for chemical reactions between the two phases. The preparation of composites by adding GDC electrolyte for SOFCs electrodes facilitates the sintering of the components of the symmetrical cell, improve the chemical stability (see SI4. Supplementary Information) and can help to minimize delamination. Additionally, by increasing the ionic conductivity of the electrode by adding GDC, the TPB length is increased and thus the electrochemical reaction sites. This improves the sintering process and leads to a lower ASR value.[9, 54, 55]

The symmetrical cells were prepared by screen-printing the electrode materials onto the commercial GDC substrates. BFCZO cells consist of BFCZO powder sintered onto a GDC electrolyte pellet, while BFCZO-GDC cells were fabricated by screen-printing BFCZO-GDC electrodes (BFCZO: GDC 70:30) onto the GDC electrolytes. Six cells were fabricated and tested in total, three BFCZO cells and three BFCZO-GDC cells.

The impedance spectroscopy spectra of two representative symmetrical BFCZO/GDC/BFCZO and BFCZO:GDC/GDC/BFCZO:GDC cells in a 2-electrode configuration from 500 °C to 800 °C are shown in Figure 7. As expected, the diameter of the semicircle is reduced by increasing the temperature in both cells, indicating a decrease of the resistance. It can also be observed that the introduction of GDC mixed with BFCZO dramatically reduces the polarization resistance, enhancing the electrochemical performance. The two resistances extracted from the semicircle diameters and the non-zero intercept of the data, the activation energy of both processes and the study of the cells stability on heating and cooling cycles are displayed in the Electronic Supplementary Information, SI4. It is shown there that the mixture of BFZCO/GDC shows improved stability of the electrochemical performance during heating/cooling cycles.

The temperature dependence of the area-specific resistance associated with the electrode polarization processes in both cells is shown in Figure 8. The observed ASR_p values in air for BFCZO cells during heating were 7.19, 3.39, 1.47, 0.66, 0.33, 0.22 and 0.13 Ω·cm² at 500, 550, 600, 650 700, 750 and 800 °C, respectively. As mentioned above, these results are further improved when GDC is added to the BFCZO electrode material and BFCZO-GDC cells were tested. The ASR_p values in air for this cell were 5.89, 2.13, 0.83, 0.33, 0.13, 0.08 and 0.05 Ω cm² at 500, 550, 600, 650, 700, 750 and 800 °C, respectively. The ASR_p for BFCZO and BFCZO-GDC cells decreases from 0.33 to 0.13 Ω cm² at 700 °C and from 0.13 to 0.05 Ω cm² at 800 °C, satisfying the condition of ASR_p lower than 0.15 Ω cm² at the application temperature.[5, 16] Some of the reported ASR_p at 700 ºC for other SOFC cathodes are 0.13 Ω·cm² for $Bi_{0.5}Sr_{0.5}Fe_{0.8}Cu_{0.2}O_{3-\delta}$,[56] 0.11 Ω·cm² for $BaCe_{0.1}Fe_{0.6}Co_{0.3}O_{3-\delta}$,[57] 0.07 Ω cm² for $(GdBa)_{0.8}Ca_{0.4}Co_{0.6}Fe_{1.4}O_{6-\delta}$,[58] 0.2 Ω·cm² for $La_{0.5}Ba_{0.5}CoO_3$,[59] 0.28 Ω·cm² for $La_{0.75}Sr_{0.25}Cr_{0.5}Mn_{0.5}O_{3-\delta}$, [60] 0.035 Ω·cm² for $Ba_{0.5}Sr_{0.5}Co_{0.8}Fe_{0.2}O_{3-\delta}$,[61] 0.035 Ω·cm² for $BaCo_{0.4}Fe_{0.4}Zr_{0.2}O_{3-\delta}$ (at 650 ºC)[51] and 0.034 Ω·cm² for $Nd_{0.5}Sr_{0.5}Co_{0.5}Fe_{0.5}O_{3-\delta}$.[62]

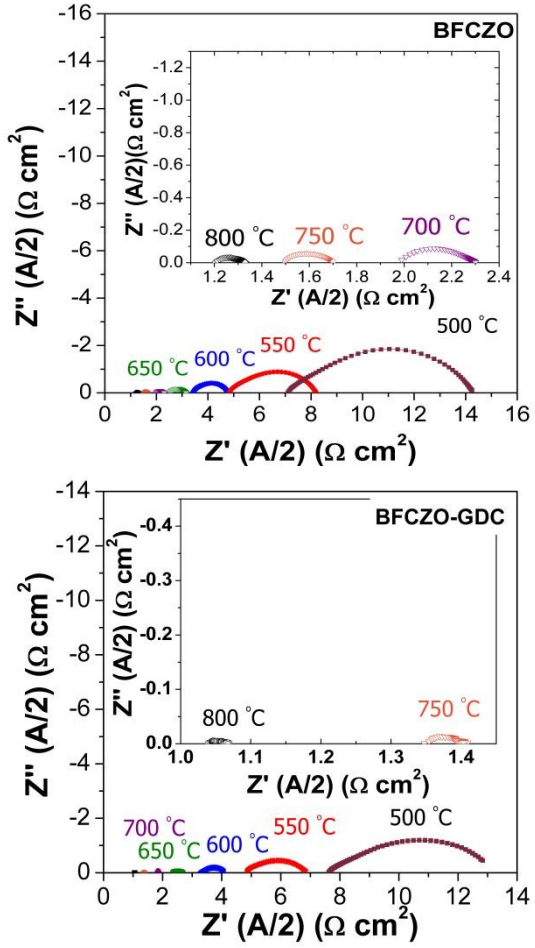

Figure 7. Impedance spectroscopy spectra of two representative symmetrical cells in a 2-electrode configuration from 500 °C to 800 °C. (a) BFCZO cell refers to BFCZO/GDC/BFCZO cell and (b) BFCZO-GDC corresponds to the BFCZO:GDC/GDC/ BFCZO:GDC symmetrical cell. The figure Insets shows a magnification of the spectra collected at 700 °C, 750 °C and 800 °C.

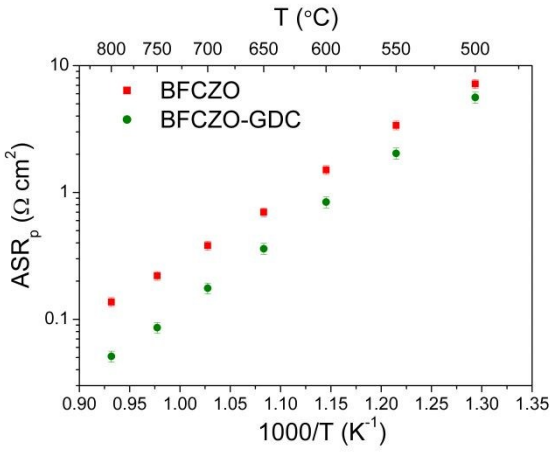

Figure 8. Temperature dependence on ASR associated with the electrode polarization processes for BFCZO cell and BFCZO-GDC cell.

Figure 9 shows a cross-sectional SEM image of a post-mortem BFCZO-GDC symmetrical cell. It can be seen that the thickness of the electrode layer is *ca.* 5 µm. The electrode material shows a porous structure as desired (Figure 9a). Furthermore, there are no signs of electrode delamination after electrochemical performance. The BFCZO-GDC material shows good contact with the GDC electrolyte after electrochemical testing (Figure 9b).

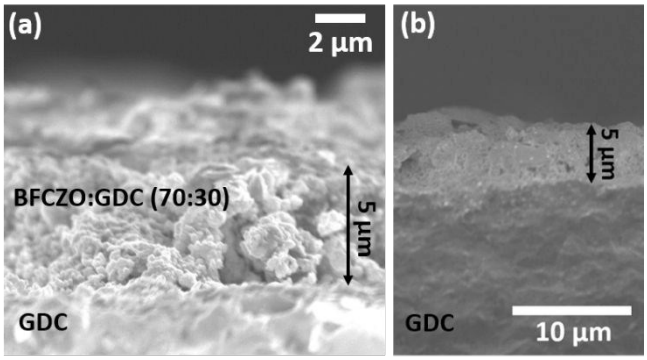

Fig 9. Cross-sectional FE-SEM view of the symmetrical cell BFCZO-GDC.

The cells described in this work were prepared manually, which still offer optimization possibilities by adjusting and controlling the deposition of the electrodes, which might improve the electrochemical performance by reducing the polarization resistance. Future work may be dedicated to the incorporation of BFCZO into fully functional IT-SOFCs and their performance testing.

Conclusions

In a nutshell, we have shown that $BaFe_{0.125}Co_{0.125}Zr_{0.75}O_{3-\delta}$ (BFCZO) is a promising cathode for IT-SOFCs. The BFCZO perovskite phase has been synthesized by the citrate method. Synchrotron X-ray diffraction, neutron diffraction and high resolution transmission electron microscopy show a cubic $Pm\bar{3}m$ phase. Neutron thermo-diffraction reveals oxygen deficiency in the sample with no signs for cation or oxygen vacancy ordering. The number of oxygen vacancies increase upon heating, from $BaFe_{0.13(1)}Co_{0.13(1)}Zr_{0.74(1)}O_{2.90(2)}$ at room temperature to $BaFe_{0.13(1)}Co_{0.13(1)}Zr_{0.74(1)}O_{2.86(1)}$ at 700 °C. The thermal expansion coefficient of 8.1 x 10^{-6} K^{-1}, determined from crystal structure analysis, suggests that the material is compatible with common electrolytes. Electrochemical impedance spectroscopy of the sintered material shows asymmetric relaxation peaks in the Modulus M" vs frequency plot, which is typical for ionic conductors. Furthermore, symmetrical cells of BFCZO show an area-specific resistance of 0.33 Ω·cm^2 at 700 °C and 0.13 Ω·cm^2 at 800 °C. These values are improved to 0.13 Ω·cm^2 at 700 °C and to 0.05 Ω·cm^2 at 800 °C by mixing 70 %wt BFCZO with 30%wt of $Ce_{0.9}Gd_{0.1}O_{2-\delta}$.

The results encountered here in this work validate the theoretical predictions of Jacobs et al.,[41] where the screening of a large amount of perovskite phases using several filters leads to viable suggestions for new materials that may be most promising for industrial use as IT-SOFC cathode materials.

Conflicts of interest

View Article Online
DOI: 10.1039/C9TA12208G

The authors declare no conflict of interests.

Acknowledgements

This research was funded by the Spanish Ministry of Science, Innovation and Universities through grants MAT2017-87134-C2-2-R MAT2017-84385-R and MAT2016-78362-C4-4R. JPG would also like to thank Community of Madrid for granting an "Atracción de Talento" fellowship (2017-T2-IND-5597). The authors wish to express their gratitude to ALBA synchrotron, ILL neutron facilities and Centro Nacional de Microscopía Electrónica (CNME) at the Universidad Complutense de Madrid (UCM). We thanks to José Antonio Alonso for useful discussion, to Jacobo Santamaría, Carlos León and Alberto Rivera-Calzada for allowing use and help with the Novocontrol impedance analyzer and to Susana García Martín for allowing use and help with the Solartron 1255 analyser.

References

1. A. Atkinson, S. Skinner and J. Kilner, *Fuel Cells and Hydrogen Production: A Volume in the Encyclopedia of Sustainability Science and Technology, Second Edition*, 2019, 569-589.
2. A. B. Stambouli and E. Traversa, *Renew. Sust. Energ. Rev.*, 2002, **6**, 433-455.
3. N. Mahato, A. Banerjee, A. Gupta, S. Omar and K. Balani, *Prog. Mater. Sci.*, 2015, **72**, 141-337.
4. W. H. Kan, A. J. Samson and V. Thangadurai, *J. Mater. Chem. A*, 2016, **4**, 17913-17932.
5. D. J. Brett, A. Atkinson, N. P. Brandon and S. J. Skinner, *Chem. Soc. Rev.*, 2008, **37**, 1568-1578.
6. A. Tarancón, S. J. Skinner, R. J. Chater, F. Hernandez-Ramirez and J. A. Kilner, *J. Mater. Chem.* , 2007, **17**, 3175-3181.
7. S. Yoo, A. Jun, Y. W. Ju, D. Odkhuu, J. Hyodo, H. Y. Jeong, N. Park, J. Shin, T. Ishihara and G. Kim, *Angew. Chem.* , 2014, **53**, 13064-13067.
8. J. A. Kilner and M. Burriel, *Annu. Rev. Mater. Res.*, 2014, **44**, 365-393.
9. K. Boulahya, D. Muñoz-Gil, A. Gómez-Herrero, M. T. Azcondo and U. Amador, *J. Mater. Chem. A*, 2019, **7**, 5601-5611.
10. Z. Zhu, M. Li, C. Xia and H. J. Bouwmeester, *J. Mater. Chem. A*, 2017, **5**, 14012-14019.
11. Z. Shao and S. M. Haile, *Nature* 2004, **431**, 255-258.
12. C. Sun, R. Hui and J. Roller, *J. Solid State Electr.*, 2010, **14**, 1125-1144.
13. R. E. Williford and P. Singh, *J. Power Sources*, 2004, **128**, 45-53.
14. P. Granger, V. I. Parvulescu, S. Kaliaguine and W. Prellier, *Perovskites and related mixed oxides: concepts and applications*, John Wiley & Sons, 2015.
15. L. Rioja-Monllor, C. Bernuy-Lopez, M.-L. Fontaine, T.

Grande and M.-A. Einarsrud, *Journal of Materials Chemistry A*, 2019, **7**, 8609-8619.
16. S. Sameshima, T. Ichikawa, M. Kawaminami and Y. Hirata, *Mater. Chem. Phys.*, 1999, **61**, 31-35.
17. F. Zhao, R. Peng and C. Xia, *Fuel Cells Bull.*, 2008, **2008**, 12-16.
18. K. Park, S. Yu, J. Bae, H. Kim and Y. Ko, *International Journal of Hydrogen Energy*, 2010, **35**, 8670-8677.
19. T. Ishihara, *Perovskite oxide for solid oxide fuel cells*, Springer Science & Business Media, 2009.
20. J. Richter, P. Holtappels, T. Graule, T. Nakamura and L. J. Gauckler, *Monatshefte für Chemie-Chemical Monthly*, 2009, **140**, 985-999.
21. D. Muñoz-Gil, D. Pérez-Coll, E. Urones-Garrote, U. Amador and S. García-Martín, *J. Mater. Chem. A*, 2017, **5**, 12550-12556.
22. E. Maguire, B. Gharbage, F. Marques and J. Labrincha, *Solid State Ionics*, 2000, **127**, 329-335.
23. O. Gwon, S. Yoo, J. Shin and G. Kim, *International Journal of Hydrogen Energy*, 2014, **39**, 20806-20811.
24. J. Van Herle, A. McEvoy and K. R. Thampi, *Electrochimica Acta*, 1996, **41**, 1447-1454.
25. H.-K. Lee, *Materials chemistry and Physics*, 2003, **77**, 639-646.
26. E. Lay, M. Benamira, C. Pirovano, G. Gauthier and L. Dessemond, *Fuel Cells*, 2012, **12**, 265-274.
27. Z. Wang, H. Zhao, N. Xu, Y. Shen, W. Ding, X. Lu and F. Li, *Journal of Physics and Chemistry of Solids*, 2011, **72**, 50-55.
28. G. Zhang, X. Dong, Z. Liu, W. Zhou, Z. Shao and W. Jin, *Journal of Power Sources*, 2010, **195**, 3386-3393.
29. Y. Guo, D. Chen, H. Shi, R. Ran and Z. Shao, *Electrochimica Acta*, 2011, **56**, 2870-2876.
30. Z. Shao and S. M. Haile, in *Materials for Sustainable Energy: A Collection of Peer-Reviewed Research and Review Articles from Nature Publishing Group*, World Scientific, 2011, pp. 255-258.
31. E. Girdauskaite, H. Ullmann, V. Vashook, U. Guth, G. Caraman, E. Bucher and W. Sitte, *Solid State Ionics*, 2008, **179**, 385-392.
32. Y. Hu, Y. Bouffanais, L. Almar, A. Morata, A. Tarancon and G. Dezanneau, *International Journal of Hydrogen Energy*, 2013, **38**, 3064-3072.
33. T. Ghorbani-Moghadam, A. Kompany, M. Bagheri-Mohagheghi and M. E. Abrishami, *Ceramics International*, 2018, **44**, 21238-21248.
34. J. Prado-Gonjal, R. Schmidt, J. Espíndola-Canuto, P. Ramos-Alvarez and E. Morán, *J. Power Sources*, 2012, **209**, 163-171.
35. Q. Liu, F. Zhao, X. Dong, C. Yang and F. Chen, *J. Phys. Chem. C*, 2009, **113**, 17262-17267.
36. A. Ferrel-Álvarez, M. Domínguez-Crespo, H. Cong, A. Torres-Huerta, S. Brachetti-Sibaja and W. De La Cruz, *J. Alloys Compd.*, 2018, **735**, 1750-1758.
37. J. Prado-Gonjal, R. Schmidt and E. Morán, *Inorganics*, 2015, **3**, 101-117.
38. B. Molero-Sánchez, J. Prado-Gonjal, D. Ávila-Brande, V. Birss and E. Morán, *Ceram. Int.*, 2015, **41**, 8411-8416.
39. M. Niederberger, N. Pinna, J. Polleux and M. Antonietti, *Angew. Chem.*, 2004, **43**, 2270-2273.
40. J. Prado-Gonjal, R. Heuguet, D. Muñoz-Gil, A. Rivera-Calzada, S. Marinel, E. Morán and R. Schmidt, *Inter. J. Hydrog. Energy*, 2015, **40**, 15640-15651.
41. R. Jacobs, T. Mayeshiba, J. Booske and D. Morgan, *Adv. Energy Mater.*, 2018, **8**, 1702708. View Article Online DOI: 10.1039/C9TA12208G
42. Y.-L. Lee, J. Kleis, J. Rossmeisl, Y. Shao-Horn and D. Morgan, *Energ. Environ. Sci.*, 2011, **4**, 3966-3970.
43. F. Fauth, I. Peral, C. Popescu and M. Knapp, *Powder Diffr.*, 2013, **28**, S360-S370.
44. J. Rodríguez-Carvajal, *Physica B: Condensed Matter*, 1993, **192**, 55-69.
45. S. B. Adler, *Solid State Ionics*, 1998, **111**, 125-134.
46. S. B. Adler, *Chem. Rev.*, 2004, **104**, 4791-4844.
47. D. Johnson, *ZView: A software Program for IES Analysis*, 2005.
48. R. Schmidt, *Ceramic Materials Research Trends*, 2007, 321.
49. J. T. Irvine, D. C. Sinclair and A. R. West, *Adv. Mater.*, 1990, **2**, 132-138.
50. C. Cuerva, J. A. Campo, M. Cano and R. Schmidt, *Dalton Trans.*, 2017, **46**, 96-105.
51. L. Zhang, J. Shan and Q. Wang, *Journal of Alloys and Compounds*, 2019, **771**, 221-227.
52. J. Lu, Y.-M. Yin and Z.-F. Ma, *international journal of hydrogen energy*, 2013, **38**, 10527-10533.
53. W. Münch, K.-D. Kreuer, G. Seifert and J. Maier, *Solid State Ionics*, 2000, **136**, 183-189.
54. J. M. Porras-Vazquez, T. Pike, C. A. Hancock, J. F. Marco, F. J. Berry and P. R. Slater, *Journal of Materials Chemistry A*, 2013, **1**, 11834-11841.
55. V. Dusastre and J. Kilner, *Solid state ionics*, 1999, **126**, 163-174.
56. L. Gao, M. Zhu, Q. Li, L. Sun, H. Zhao and J.-C. Grenier, *Journal of Alloys and Compounds*, 2017, **700**, 29-36.
57. L. Zhang, J. Li, J. Yang and H. Shen, *Electrochimica Acta*, 2015, **154**, 244-248.
58. X. M. de Irujo-Labalde, D. Muñoz-Gil, E. Urones-Garrote, D. Ávila-Brande and S. García-Martín, *Journal of Materials Chemistry A*, 2016, **4**, 10241-10247.
59. A. E. M. Gómez, D. G. Lamas, A. G. Leyva and J. Sacanell, *Ceramics International*, 2019.
60. J. Peña-Martínez, D. Marrero-López, D. Pérez-Coll, J. Ruiz-Morales and P. Núñez, *Electrochimica acta*, 2007, **52**, 2950-2958.
61. S. Lee, Y. Lim, E. A. Lee, H. J. Hwang and J.-W. Moon, *Journal of Power Sources*, 2006, **157**, 848-854.
62. X. Zhu, C. Qian, F. Sun, L. Zhang, X. Liu and D. Li, *Journal of Alloys and Compounds*, 2019.

Table of contents

View Article Online
DOI: 10.1039/C9TA12208G

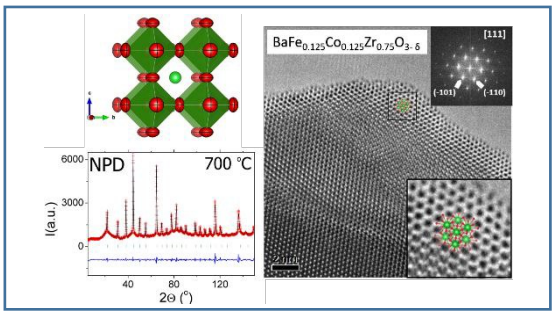

$BaFe_{0.125}Co_{0.125}Zr_{0.75}O_{3-\delta}$ perovskite is a novel and efficient MIEC electrode for intermediate-temperature solid oxide fuel cells. Symmetrical cells with an area-specific resistance of 0.13 $\Omega \cdot cm^2$ at 700 °C and 0.05 $\Omega \cdot cm^2$ at 800 °C have been prepared.